

# Update of LOCA-Integral and POST-LOCA-Bend Test Results for Fresh ZIRLO Cladding

Y. Yan, T.A. Burtseva, R.O. Meyer, and M.C. Billone  
Argonne National Laboratory

July 21, 2010

## Summary of Results

Detailed results for 18 LOCA integral tests and 11 post-LOCA bend tests were documented in a February 9, 2010 letter report (“Post-LOCA Bend Test Results for As-fabricated Cladding,” by Y. Yan, T.A. Burtseva, R.O. Meyer, and M.C. Billone) sent to NRC. The purpose of this update is to document the results of an additional 8 LOCA tests and 5 post-LOCA bend tests. Table 1 lists the results described in the Feb. 9<sup>th</sup> letter report. Some adjustments have been made to the rupture strain, which is defined in this work as the increase in cladding mid-wall circumference ( $\Delta C_m = C_{mf} - C_{mi}$ ) normalized to the initial mid-wall circumference ( $C_{mi} = 28.05$  mm for 17×17 ZIRLO cladding). For rupture strains listed in bold red (OCZL#7, #11, and #19),  $C_{mf}$  was measured from 25X composite images of the cross section through the mid-span of the rupture opening. All other rupture strains in Table 1 were calculated from an empirical relationship (see next paragraph) for the final mid-wall circumference ( $C_{mf}$ ) as a function of measured diameters at two orientations and rupture-opening width.

The results generated since Feb. 9<sup>th</sup> are summarized in Table 2. For three of these ballooned-and-ruptured LOCA samples (OCZL#25, #29, and #30), the circumference of the outer-cladding surface ( $C_{of}$ ) was measured directly and converted to  $C_{mf}$  by accounting for the small reduction due to the average cladding thickness. These rupture strain values are listed in bold red. An empirical relationship was derived to determine  $C_{mf}$  as a function of the average of the maximum (rupture tips to back of cladding,  $D_{max}$ ) and minimum (90° from rupture opening,  $D_{min}$ ) outer diameters ( $D_{avg} = [D_{max} + D_{min}]/2$ ) and the rupture width ( $\delta_R$ ):  $C_{mf} = \pi (D_{avg} - 0.333 \delta_R)$ , where the empirical factor 0.333 gave the best fit to the 6 measured  $C_{mf}$  values. The variation of rupture strain with rupture temperature is shown in Fig. 1. By comparing these results to the well-publicized results for Zry-4, it is clear Nb-containing ZIRLO has a lower alpha to alpha-plus-beta phase transition temperature than the 810°C for as-fabricated Zry-4. However, not enough data were obtained for ZIRLO rupture temperatures in the range of 700±25°C to determine the temperature shift for the alpha strain peak and for the phase change.

Three metrics have been used to assess the post-LOCA performance of ZIRLO subjected to four-point-bend tests: maximum bending moment, which is a measure of strength; failure energy, which is a measure of material toughness; and plastic displacement, which is a measure of ductility. The maximum bending moment is determined from the load-displacement curve according to  $M_{max} = (0.05 \text{ m}) (P_{max}/2)$  where 0.05 m is the distance between the support and the loading point (net moment arm),  $P_{max}/2$  is the load each of the two supports, and  $P_{max}$  is the maximum recorded load. Failure energy (or maximum energy through 14-mm displacement for non-failed samples) is determined from the area under the load-displacement curve, which is calculated numerically. Plastic displacement is determined by the standard offset displacement method.

The maximum bending moment decreases with oxidation level expressed as % CP-ECR (see Fig. 2). The decrease is essentially linear from 10% to 18% CP-ECR, with a small non-linearity between 0% and 10% CP-ECR. Within expected data scatter, it appears that the results are independent of rupture strains in the range of 20% to 50%.

The maximum energy is dependent on the width (150 mm) of the span exposed to the uniform bending moment. To generalize the results, the maximum energy is normalized to the maximum energy of the highly ductile 0% CP-ECR samples that were subjected to 14-mm displacement at 2 mm/s and 135°C. Figure 3 shows the measured energy normalized to 20.75 J as a function of CP-ECR. The results show a very steep drop between 0% and 10% CP-ECR and a more gradual linear decrease between 10% and 18% CP-ECR. These results also appear to be independent of rupture strain.

Based on benchmark tests with as-fabricated M5 and tests with ballooned and ruptured ZIRLO at 0% CP-ECR, the offset displacement method for determining plastic deformation is straightforward and reliable. None of these samples cracked during the 14-mm displacement applied at the loading points. It was also demonstrated from loading-unloading benchmark tests that the loading slope was equal to the unloading and reloading slope. Therefore, deviation from linear behavior did represent the plastic deformation of the sample. However, most load-displacement curves for oxidized, ballooned-and-ruptured samples showed linear elastic behavior followed by a very steep load drop to zero. This load drop corresponded to severing of the cross section through the rupture region (for rupture strains >30%) or to severing at locations above and below the rupture length in the higher hydrogen regions (for  $\leq 30\%$  rupture strain). For samples that severed in the higher-hydrogen regions away from the rupture opening, brittle failure (i.e., severing of the sections with no offset strain) occurred. This result was consistent with ring-compression test results for pre-hydrided and high-burnup cladding samples. For samples that severed in the rupture-node cross section, the failures appeared to be brittle in the sense that no plastic deformation was observed prior to crack initiation and the drop in load to zero was very steep. For oxidized LOCA integral samples, the local oxidation level varies from about 100% at the rupture tips to less than the average value (e.g., <12% CP-ECR for OCZL#18) 180° from the rupture opening. With the rupture tips under maximum tensile stress, the crack initiated at these tips and propagated rapidly through the brittle and “ductile” regions of the cross section with no load-displacement-curve indication of plastic flow. While most of the cladding cross section would exhibit high ductility in the absence of a flaw, the material does not have enough local ductility (i.e., fracture toughness) to blunt crack growth. There were a few samples that did indicate macroscopic plastic flow prior to 90-100% severing of the cross section. Results from these test samples are discussed in detail in the next section.

It should be emphasized that all of the ZIRLO samples and the Zry-2 samples (see NUREG/CR-6967, Section 6) survived oxidation to  $\leq 20\%$  CP-ECR and quench without fragmentation or crack initiation. The post-LOCA bend tests demonstrate that additional strength and toughness remain in the balloon region beyond what is needed to survive the thermal stresses during unrestrained quench.

Table 1. Summary of results for LOCA integral and post-LOCA bend tests with as-fabricated ZIRLO cladding. The reference LOCA test conditions are: 1200-psig pressure at 300°C, 5°C/s heating rate to 1200°C, 1200°C hold temperature, 3°C/s cooling rate to 800°C, and quench at 800°C. Samples OCZL#8-11 are from ramp-to-burst tests that were slow-cooled without quench.

Test ID OCZL#	Fill Pressure, psig	Rupture Strain, % (T <sub>R</sub> , °C)	CP-ECR %	Quench at 800°C	Stress in Rupture Node	Failure Location	Maximum Bending Moment N•m	Maximum Energy J	Plastic Displ. mm
6	1200	41 (750±30)	18	No	---	---	---	---	---
7	800	<b>22</b> (810±30)	16	No	---	---	---	---	---
8	600	19 (845±25)	0	No	Maximum tension	No cracking	20.9	>8.4	>7.7
9	400	33 (875±15)	0	No	Maximum tension	No cracking	20.6	>8.3	>7.7
10	1600	68 (715±10)	0	No	Maximum tension	No cracking	19.5	>7.7	>7.1
11	1400	<b>40</b> (≈750)	0	No	---	---	---	---	---
12	1000	31 (805±20)	14	No	Maximum compression	-40 mm +33 mm	10.5	0.78	0
13	1200	41 (741±15)	14	No	Maximum tension	Rupture opening	8.8	0.58	0
14	1200	46 (735±6)	18	Yes	Maximum tension	Rupture opening	5.7	0.24	0
15	1200	50 (755±23)	18	Yes	Maximum compression	Cracking; no failure	8.9	>2.3	>13
17	1200	47 (750±17)	13	Yes	Maximum tension	Rupture opening	8.4	0.71	> 6.3
18	1200	<b>43</b> (748±4)	12	Yes	Maximum tension	Rupture opening	13.5	1.29	0

Table 2. Additional LOCA integral and post-LOCA bend tests with as-fabricated ZIRLO cladding. Reference LOCA conditions for these tests were: 600-psig or 1200-psig fill pressure at 300°C, 5°C/s heating rate to 1200°C, 1200°C hold temperature, 3°C/s cooling rate to 800°C, and quench at 800°C. Reference conditions for bending tests were 2 mm/s displacement rate to 14-mm maximum displacement. The displacement rate was lowered to 1 mm/s after the OCZL#21 bend test to more closely approximate ring-compression maximum strain rate and axial-bend maximum strain rate.

Test ID OCZL#	Fill Pressure, psig	Rupture Strain, % (T <sub>R</sub> , °C)	CP-ECR %	Quench at 800°C	Stress in Rupture Node	Failure Location	Maximum Bending Moment N•m	Maximum Energy J	Plastic Displ. mm
19	600	23 (840±12)	17	Yes	Maximum tension	+23 mm -23 mm	5.7	0.23	0
21	600	25 (850±10)	10	Yes	Maximum tension	+33 mm -29 mm	13.8	1.17	0
22 <sup>a</sup>	600	20 (837±12)	11	Yes	Maximum tension	+25 mm -27 mm	11.1	0.83	0
25 <sup>a</sup>	1200	<b>42</b> (757±21)	16	Yes	Maximum tension	-26 mm +26 mm	8.3	0.50	0
26	1200	31 (765±39)	16	Yes	---	---	---	---	---
27	1200	38 (760±23)	17	Yes	---	---	---	---	---
29	1200	<b>49</b> (746±19)	17	Yes	Maximum tension	Rupture opening	4.7	0.40	>8.5
30	1200	<b>42</b> (746±19)	16	Yes	Unknown <sup>b</sup>	-28 mm +48 mm	---	---	---

<sup>a</sup>Displacement rate lowered to 1 mm/s to achieve better agreement between bend and ring-compression tests for the maximum elastic strain rate.

<sup>b</sup>Sample failed at two locations during disassembly.

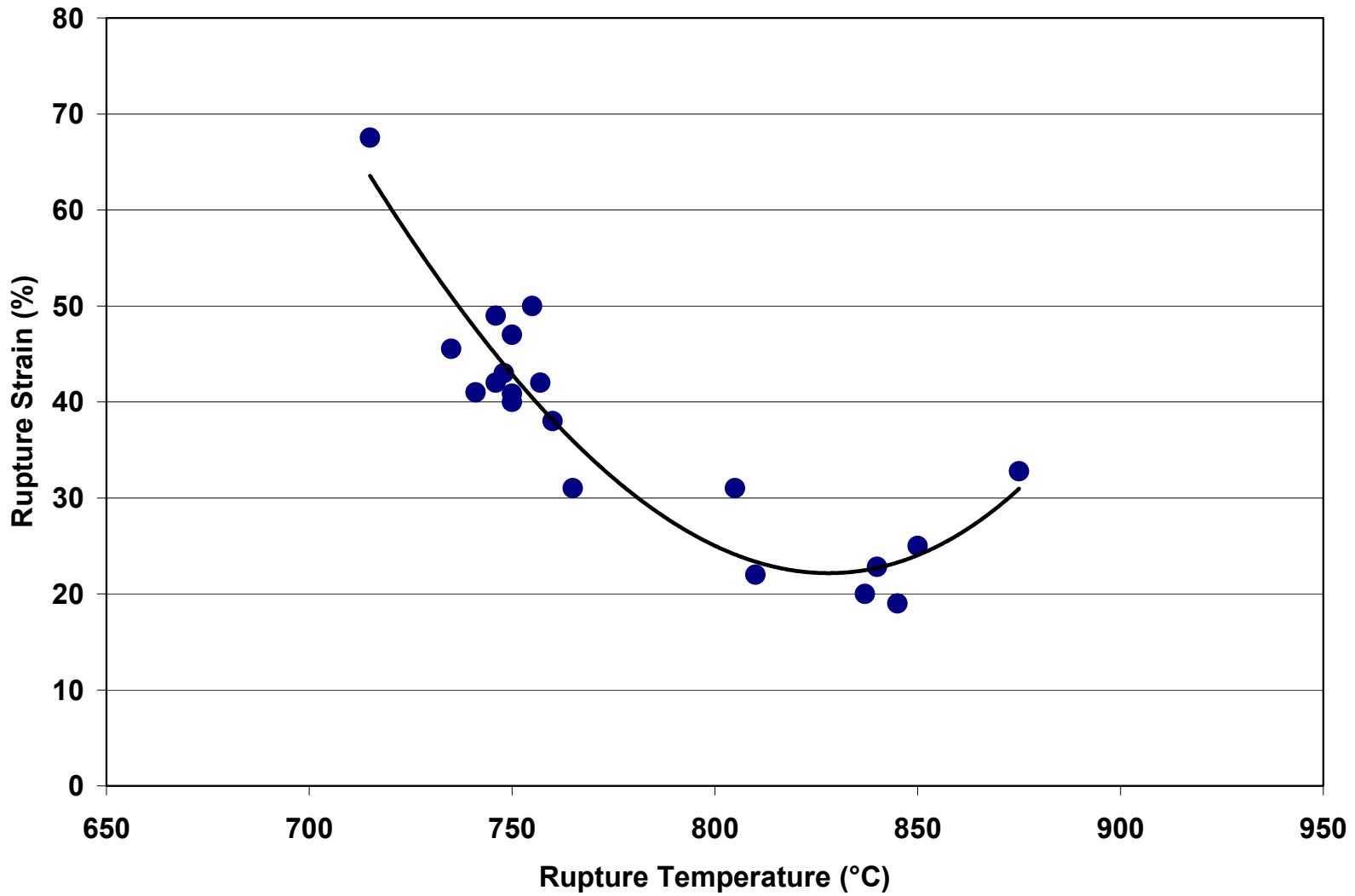


Fig. 1. Rupture strain as a function of rupture temperature for as-fabricated ZIRLO with fill pressures of 400 to 1600 psig at 300°C subjected to a temperature ramp of 5°C/s. Rupture strain is defined as the percent increase in mid-wall circumference following rupture and slow-cooling to room temperature.

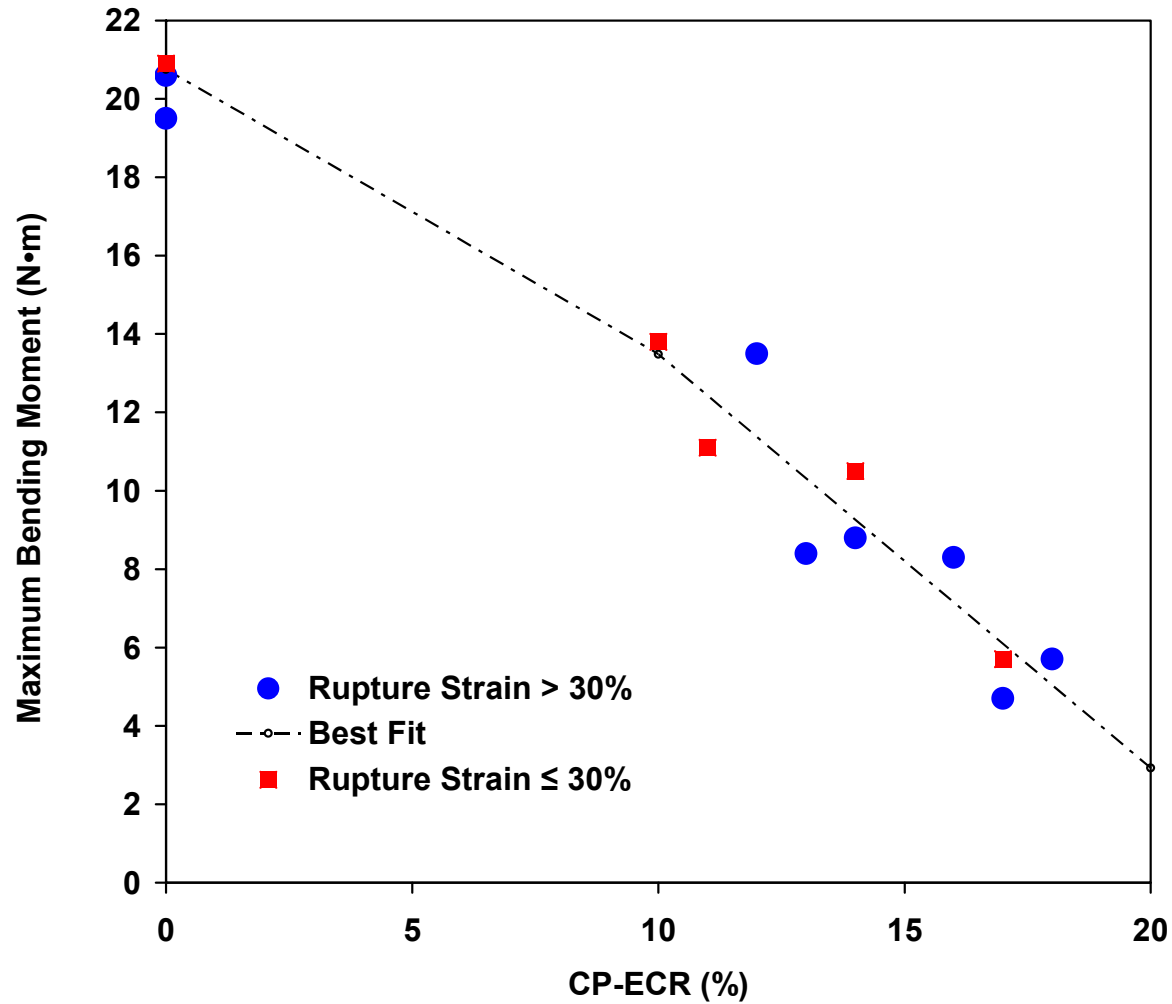


Fig. 2. Maximum bending moment as a function of oxidation level (CP-ECR) for post-LOCA samples subjected to four-point bending with the rupture region in tension for all tests but one. Bend tests were performed at 135°C and 2 or 1 mm/s to 14-mm maximum displacement.

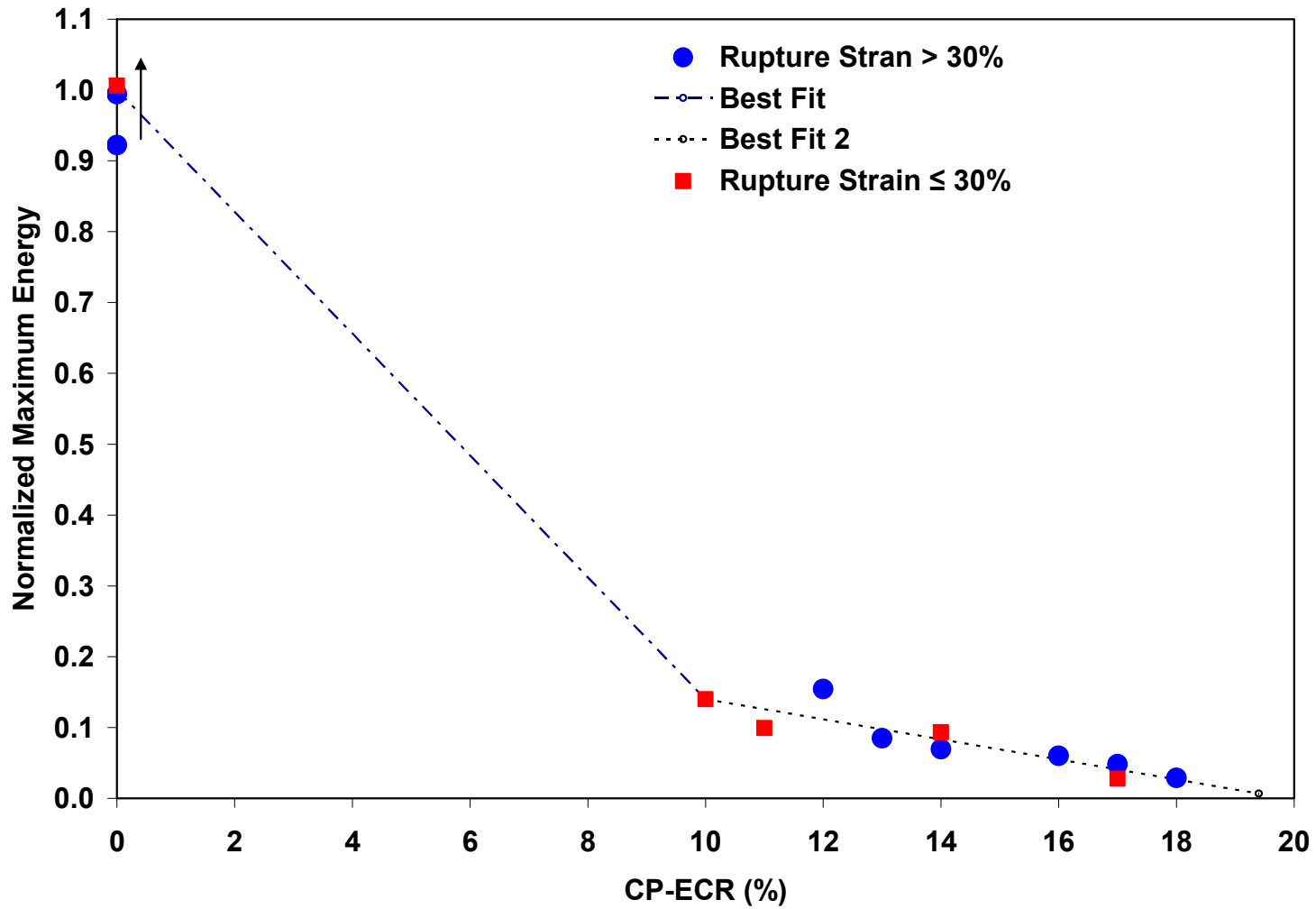


Fig. 3. Normalized maximum energy as a function of oxidation level (CP-ECR) for post-LOCA samples subjected to four-point bending with the rupture region in tension for all tests but one. Bend tests were performed at 135°C and 2 or 1 mm/s to 14-mm maximum displacement.

## Discussion

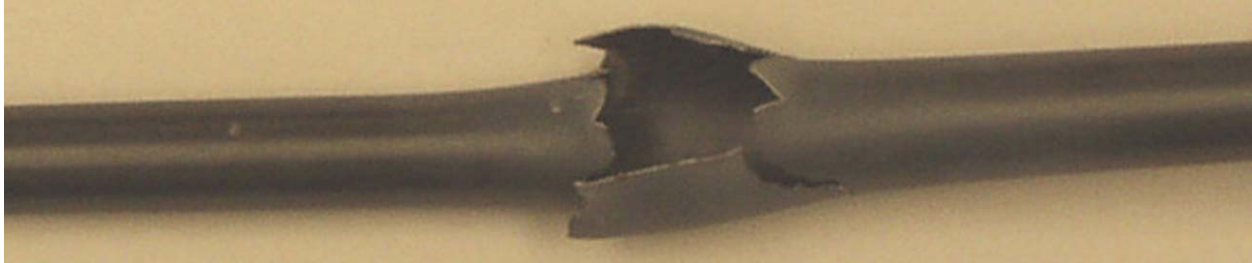
The 4-point-bend test is designed to apply a uniform bending moment between the loading points (150-mm span). Such unbiased loading allows the post-LOCA sample to fail at the weakest location. For all tests conducted with the rupture tips under maximum tensile loading, the failures occurred either in the rupture node (high oxidation level, no hydrogen pickup) or at two locations within  $\pm 50$  mm of the rupture mid-span (high hydrogen content, lower oxidation level). Prior to bending the OCZL#25 sample, the data trend indicated that samples with  $<31\%$  rupture strain severed at two locations outside the rupture region, while samples with  $>40\%$  rupture strain severed in the rupture region. However, the OCZL#25 sample (16% CP-ECR) severed at two locations outside the rupture region even though the rupture strain was high (42%) and the rupture width was large (8.7 mm). The OCZL#29 companion sample (17% CP-ECR), with a rupture strain of 49% and a rupture opening of 5.9 mm, cracked through 90% of the cross section containing the rupture opening. Metallography will be performed at the two rupture-node locations to determine why the OCZL#25 rupture-node cross section survived a bending moment of 8.3 N•m without cracking while cracking in the OCZL#29 rupture node initiated at a lower bending moment of (4.7 N•m). Figures A.4 and A.5 in Appendix A show the load-displacement curves for these two bend samples.

Macroscopic plastic flow was observed within the rupture-node cross section in the OCZL#15 sample. This sample was oriented such that the strong, ductile back region was exposed to the maximum tensile bending stress. The brittle rupture tips and surrounding material were under compression. In the absence of a crack growing through a tensile stress field, the sample survived 14-mm displacement without severing and with a plastic displacement of 13 mm (see Fig. 4). Two other tests, which were conducted with the rupture region under tension, survived the test without complete severing of the rupture-node cross-section. The OCZL#17 sample at 13% oxidation level survived 10-mm displacement with 10% of the cross section intact and a plastic displacement of 6.3 mm (see Fig. 5). The OCZL#29 sample at 17% CP-ECR exhibited plastic displacement of about 0.5 mm through the first loading phase of the test (up to  $\approx 3$  mm displacement). The sample was examined after test interruption. The crack extended through about 60% of the cross section (see Figs. 6a and 6b). After reloading, the sample exhibited ductile crack growth through 10 mm of displacement with about 10% of the cross section intact at the end of an additional 8 mm of plastic displacement (see Fig. 6c).

Post-bend-test characterization included metallographic imaging at failure locations and measurement of hydrogen-content profiles. Oxygen-content analyses are currently in progress. Figure 7a shows the hydrogen-content profile for the OCZL#12 sample that failed at locations outside the rupture region (40 mm below and 33 mm above the rupture mid-span). These failure locations are between the hydrogen peaks and the longitudinal edges of the rupture. The hydrogen content at the failure locations (1700 wppm), along with the measured circumferential strain and ECR, are shown in Fig. 7b. A low-magnification metallographic image of the severed cross section at -40 mm is shown in Fig. 7c. The outer- and inner-surface oxide layers were measured to be:  $33 \pm 5$   $\mu\text{m}$  and  $10 \pm 3$   $\mu\text{m}$ , respectively, at -40 mm; and  $32 \pm 4$   $\mu\text{m}$  and  $12 \pm 3$   $\mu\text{m}$ , respectively, at +33 mm. The metal layer thicknesses prior to oxidation were calculated to be 0.50 mm at -40 mm and 0.53 mm at +33 mm. Based on the data, it appears that these locations severed simultaneously.



(a) Low magnification side view



(b) Higher magnification rupture view

Fig. 4. Post-bend photographs of OCZL#15 LOCA sample oxidized to 18% CP-ECR and cooled with quench. The sample was bent at 135°C to 14-mm displacement with the rupture region subjected to the maximum axial compressive stress.

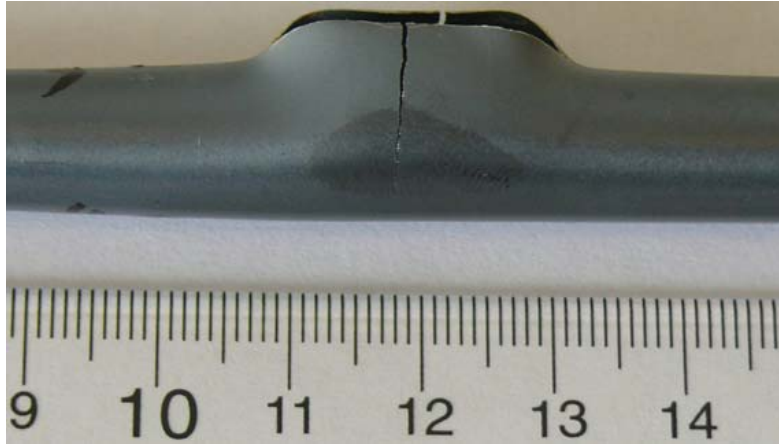


(a) Higher magnification side view

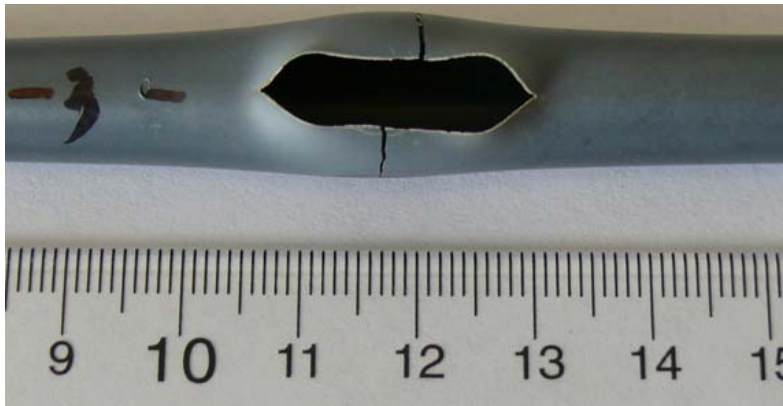


(b) Higher magnification rupture view

Fig. 5. Post-bend photographs of OCZL#17 sample (13% CP-ECR and quenched) after 10-mm displacement at 135°C with the rupture region subjected to maximum tensile stress.



(6a) Higher magnification side view after 1<sup>st</sup> loading

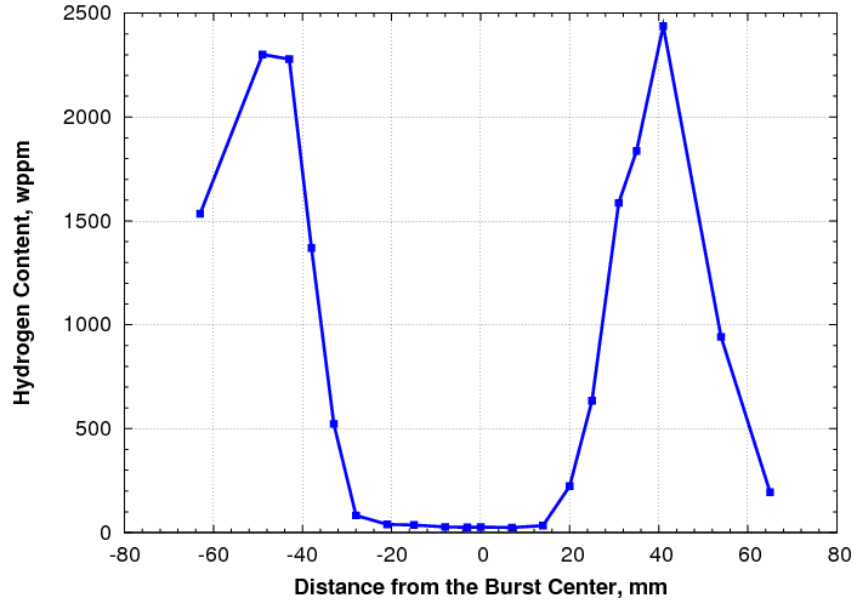


(6b) Higher magnification rupture view after 1<sup>st</sup> loading

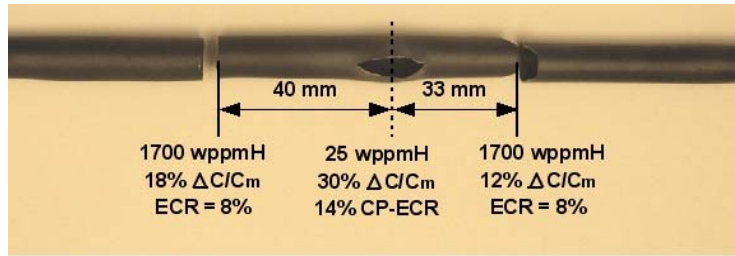


(6c) Higher magnification rupture view after 2<sup>nd</sup> loading

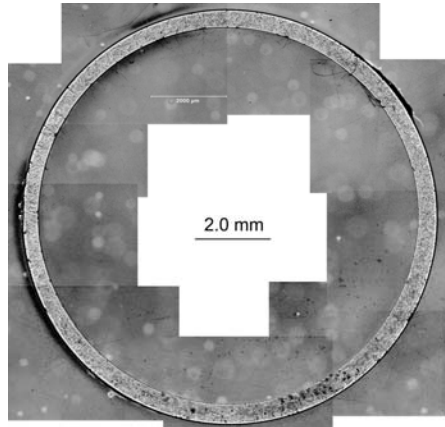
Fig. 6. Post-bend photographs of OCZL#29 sample (17% CP-ECR and quench) after 1<sup>st</sup> loading to  $\approx 3$ -mm displacement at 135°C: (a) side view and (b) rupture view; and (c) rupture view after 2<sup>nd</sup> loading to an additional 10-mm displacement at 135°C.



(a) Hydrogen-content profile



(b) Measured values at failure locations



(c) Low-magnification image of severed cross section at -40 mm

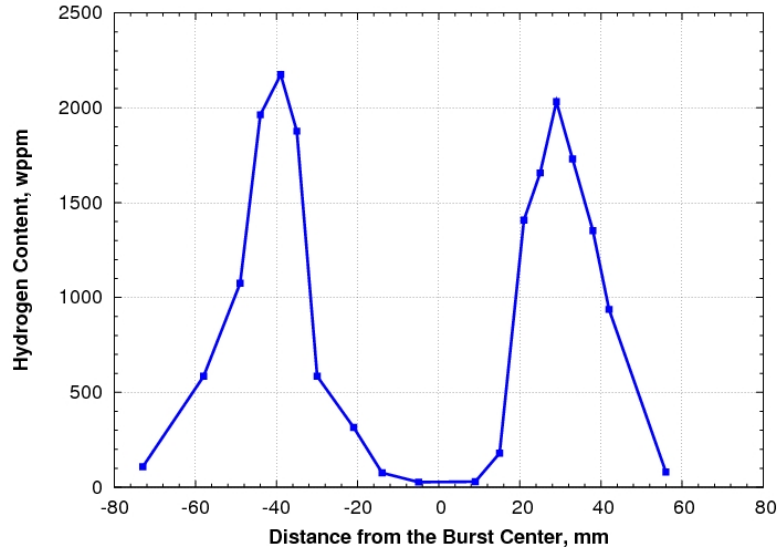
Fig. 7. Post-bend characterization of OCZL#12 sample that was subjected to bending at 135°C with the rupture region under maximum compressive stress: (a) hydrogen-content profile; (b) measured values at failure locations; and (c) low-magnification image of severed cross section at 40 mm below rupture mid-span.

Similar post-bend characterization was performed for the OCZL#19 sample following oxidation to 17% CP-ECR and quench at 800°C. The sample was subjected to bending with the rupture node under maximum tensile stress. Figure 8a shows the axial profile of hydrogen content. The profile is very similar to the one for the OCZL#12 sample. As shown in Fig. 8b, the sample severed at axial locations 24 mm below and above the rupture mid-span. Neither of these locations coincides with a hydrogen peak. The hydrogen content and measured ECR at the -24 mm location were 530 wppm and 12%, respectively. Based on ring-compression tests, this combination of hydrogen content and oxidation level would lead to brittle failure. The outer- and inner-surface oxide layers were measured to be  $50\pm 6$   $\mu\text{m}$  and  $35\pm 6$   $\mu\text{m}$  and the pre-oxidation metal wall thickness was determined to be 0.51 mm at the -24 mm location.

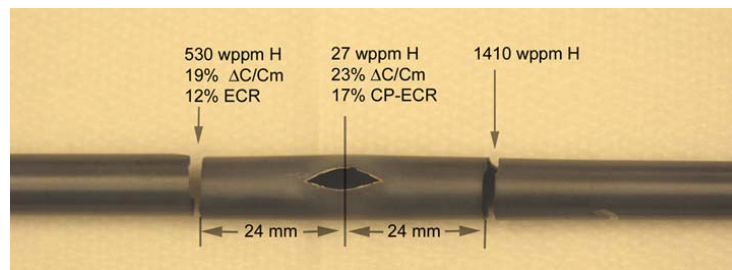
Based on similarities between the OCZL#19 and OCZL#12 sample failures, it appears that the OCZL#12 sample would have failed at the same locations even if it had been subjected to bending with the rupture region under maximum tensile stress.

The hydrogen-content profile (see Fig. 9a) was also determined for the OCZL#18 sample with 43% rupture strain and 12% CP-ECR. As indicated in Fig. 9b, the sample severed in the cross section containing the rupture node. The low magnification image of the severed cross section is shown in Fig. 9c. There was very good circumferential uniformity in oxide layer thickness ( $29\pm 1$   $\mu\text{m}$ ) based on outer- and inner-surface measurements at 10 locations. Also, the weight gain determined from metallography ( $5.40$   $\text{mg}/\text{cm}^2$ ) was very close to the CP-predicted weight gain ( $5.60$   $\text{mg}/\text{cm}^2$ ) at this location. The average metal wall thickness of the oxidized cladding was 0.35 mm. This converts to a pre-oxidation thickness of 0.39 mm. The measurements are very accurate for each image, but the 10 images represent only about 25% of the cross section. The mid-wall circumference measured from the low-magnification image was 40.0 mm. Assuming conservation of area, the pre-oxidation thickness was calculated to be  $h_f = h_i / (C_{mf} / C_{mi}) = 0.57\text{-mm} / (40.0 / 28.05) = 0.57\text{-mm} / 1.43 = 0.40$  mm. It is encouraging that the two results are very close to each other such that the CP-ECR rounds off to the same integer value of 12% using both approaches.

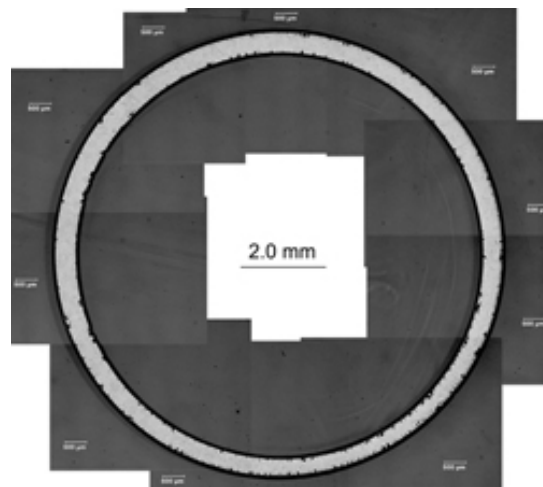
The regions of thinnest (rupture tip) and thickest (back side) cladding metal for the OCZL#18 sample are shown in Figs. 10a and 10b, respectively. It is clear from the metallography that the rupture tips are brittle and that a crack could initiate at these tips and grow into a tensile stress field. However, it is not clear why the crack would not arrest before it reached the back wall of the cladding, which should have a high ductility at <10% CP-ECR. Based on the load-displacement curve (see Fig. 11), it appears that the crack propagated rapidly through the cross section resulting in the severed sample. Although the measured offset displacement is 0.35 mm, it is not at all clear that this offset strain is due to plastic deformation in the mid-span rupture node cross section. It may be due to crack initiation (first small load drop at about 3 mm) and some crack extension (at about 4.2 mm) prior to catastrophic failure. Or it may be due to some slight slippage in the load-train. The observation that the linearized slope remains the same following the first small load drop suggests that the two points exhibiting a slight deviation from linearity do not represent plastic deformation.



(a) Hydrogen-content profile

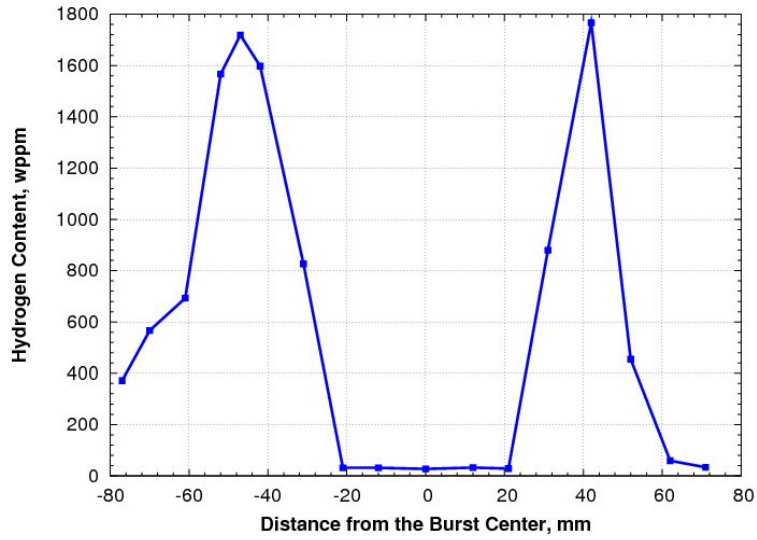


b) Measured values at failure locations



(c) Low-magnification image of severed cross section at -24 mm

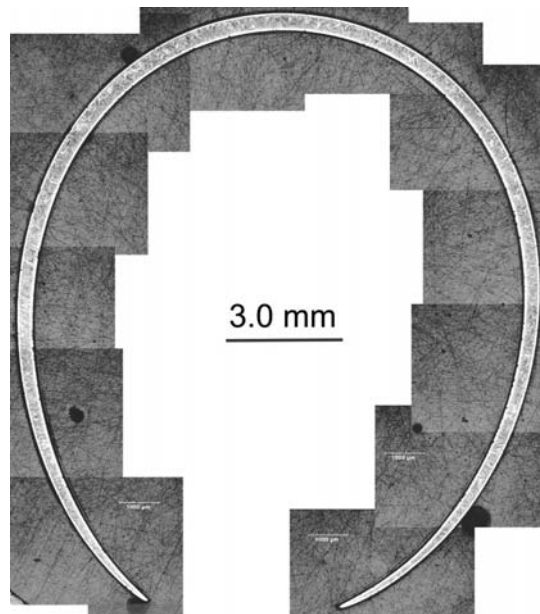
Fig. 8. Post-bend characterization of OCZL#19 sample that was subjected to bending at 135°C with the rupture region under maximum tensile stress: (a) hydrogen-content profile; (b) measured values at failure locations; and (c) low-magnification image of severed cross section at 24 mm below rupture mid-span.



(a) Hydrogen-content profile

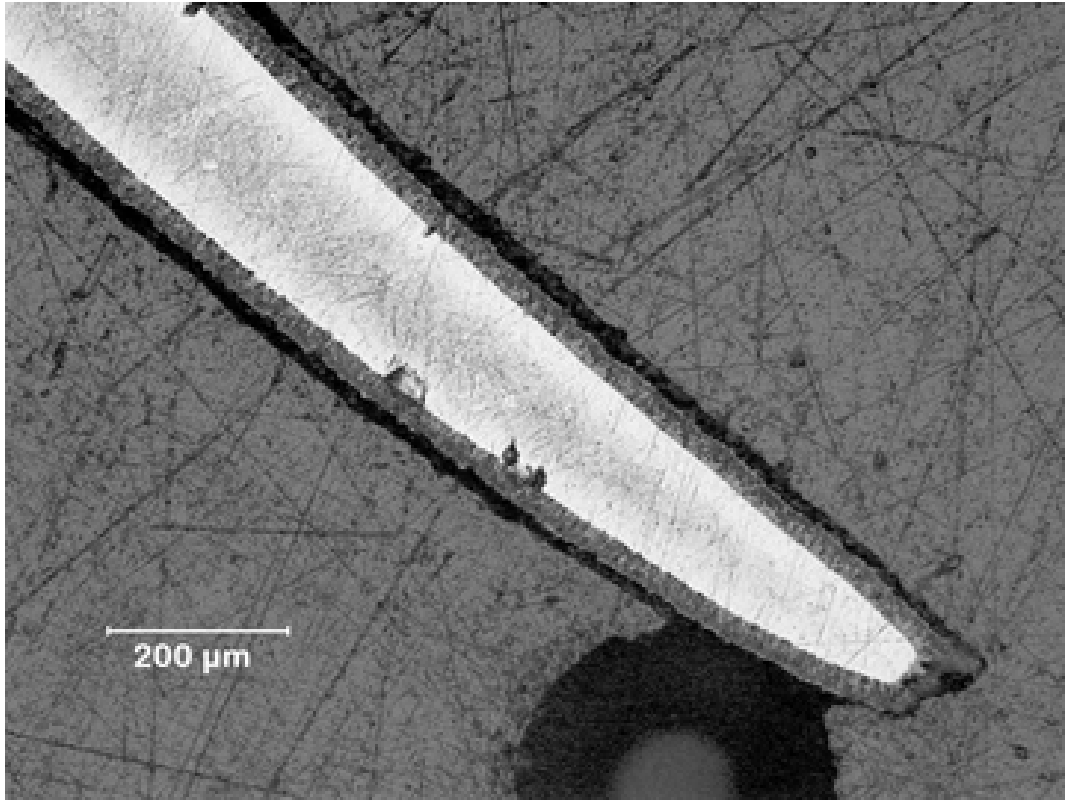


(b) Failure location

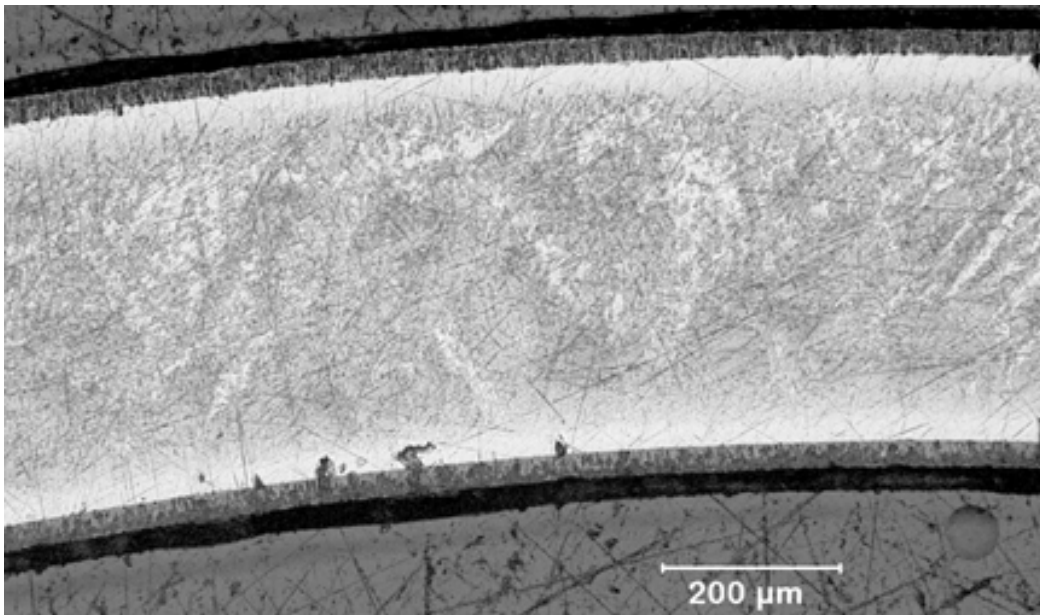


(c) Low-magnification image of severed cross section

Fig. 9. Post-bend characterization of the OCZL#18 sample oxidized to 12% CP-ECR, quenched, and subjected to bending at 135°C with the rupture region under maximum tensile stress: (a) hydrogen-content profile; (b) failure location; and (c) low-magnification image of the severed cross section.



(a) Rupture tip



(b) Back side of rupture node cross section

Fig. 10. Metallographic images for the OCZL#18 severed cross section following oxidation to 12% CP-ECR, quench, and bending at 135°C with the rupture region under maximum tension: (a) rupture tip with 0.14-mm average metal wall; and (b) back side of cross section with 0.44-mm metal wall thickness.

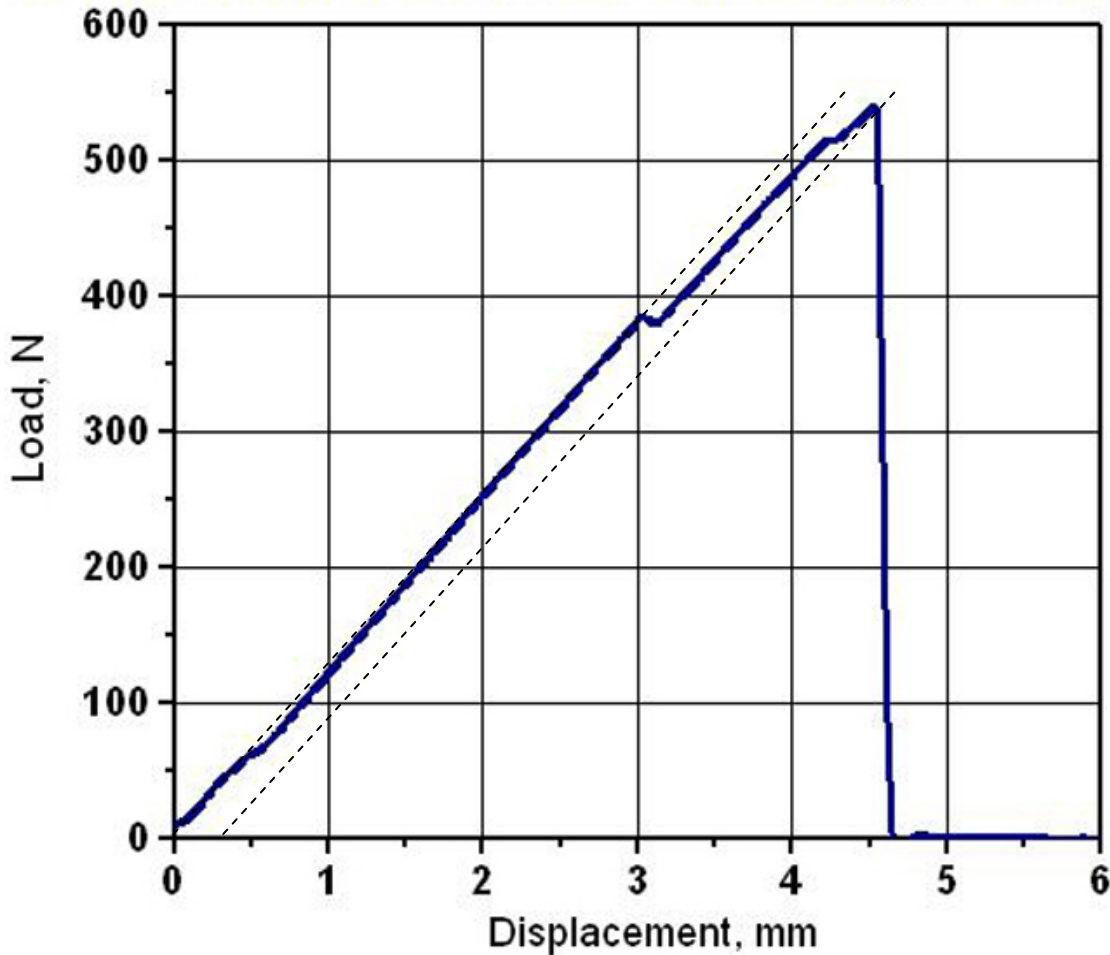


Fig. 11. Load-displacement curve for the OCZL#18 sample (12% CP-ECR and quench) during bend test at 2 mm/s and 135°C with the rupture region under maximum tensile stress.

It would have been interesting to explore the oxidation-level region from 0% to 12% for LOCA samples with >40% rupture strain. However, it is not possible to achieve <12% CP-ECR for a peak oxidation temperature of 1200°C because of the relatively thin cladding and the oxidation that occurs during the 5°C/s temperature ramp from 1000°C to 1200°C and during the cooling ramp of 3°C/s from 1200°C to 1000°C. Instead of lowering the peak oxidation temperature to achieve lower oxidation levels, an unpressurized LOCA sample was subjected to one-sided oxidation to 17% CP-ECR. The as-fabricated ZIRLO sample was held at 1186±14°C for about 890 s to achieve 17% CP-ECR. The CP-calculated outer-surface oxide layer, based on the temperature histories of the four thermocouples (TCs), was 98±6 μm. The advantage of such a sample is that ballooning, rupture, and secondary hydriding are eliminated. The ductility for such a bend sample is based on the oxygen content of the prior beta layer. ZIRLO rings oxidized to 17% CP-ECR and subjected to ring-compression tests (RCTs) exhibited relatively low offset displacements and strains of 0.39±0.14 mm and 4.1±1.5%, respectively. The corresponding permanent displacements and strains were 0.18±0.07 mm and 1.9±0.7%, respectively.

Figure 12 shows the load-displacement curve for the one-sided-oxidized, 17% CP-ECR sample subjected to 4-point bending at 135°C and 1 mm/s displacement rate. There is a clear non-linear region of the load-displacement curve prior to rapid crack growth resulting in sample severing at two locations  $\pm 38$  mm from the center of the sample. The gradual non-linearity led to an offset displacement of 0.4 mm, which is indicative of plastic deformation. It should also be noted that the failure bending moment (24.1 N•m) and failure energy (4.15 J) were factors of 4 and 18 higher, respectively, than ballooned, ruptured, and oxidized sample OCZL#19 with 23% rupture strain and 17% CP-ECR.

The remaining 76 mm of material between the two failure locations was sectioned to produce one metallographic sample and three 8-mm-long rings for ring-compression testing. Figure 13 shows the region from which the met and ring samples were sectioned. Given that the sectioned rings had already undergone plastic deformation in the axial direction, the expectation was that these rings would exhibit very low ductility or be brittle. The results of the characterization and ring-compression tests are listed in Table 3. The measured oxide thickness, based on 8 circumferential locations, was  $103 \pm 9$   $\mu\text{m}$ , which is in reasonable agreement with the CP-calculated  $98 \pm 6$   $\mu\text{m}$  based on 4 TC locations. Based on the RCT results in Table 3, the ring with 1.2% permanent strain is classified as ductile ( $\geq 1\%$ ) and the rings with 0.7% and 0.8% permanent strains are classified as brittle. On average, the post-bend material was brittle.

The relationship between post-quench bending strength and axial loads (e.g., JAEA 540 N) will be presented in an upcoming letter report (“Post-LOCA Test Methods”), which is in progress.

## Conclusions

Based on the decrease in maximum bending moment (i.e., strength) and maximum energy (i.e., toughness) with increasing oxidation level shown in Figs. 2 and 3, respectively, it is clear that the maximum oxidation level should be limited in the balloon region to increase the probability that fresh fuel rods will maintain their geometry during quench and post-quench in response to loads beyond those associated with thermal stresses in an unconstrained rod. All of the ANL LOCA integral samples (unconstrained) oxidized and quenched at  $\leq 20\%$  CP-ECR survived quench, as expected. As oxidation temperatures above 1200°C would result in enhanced decreases of maximum bending moment and energy with increasing oxidation level, it is also clear that the peak cladding temperature in the balloon region should be limited.

However, “ductility” in a ballooned, ruptured, and oxidized fuel rod is difficult to define and measure. Treating the 4-point-bend sample as a structure, most of the bend-test samples failed with no indication of macroscopic plastic deformation prior to severing of the cross section. This was expected for samples that severed in the higher hydrogen regions outside the rupture opening. For samples that severed along a cross section containing the rupture opening, most of the failures occurred with no indication of macroscopic plastic flow prior to crack initiation at the brittle tips surrounding the rupture opening. Only two of the samples appeared to have had enough “toughness” to blunt the crack prior to complete severing of the cross section. Based on ring-compression results and one reverse-bend test, there is little doubt that at least half of these cross sections experienced ductile crack growth.

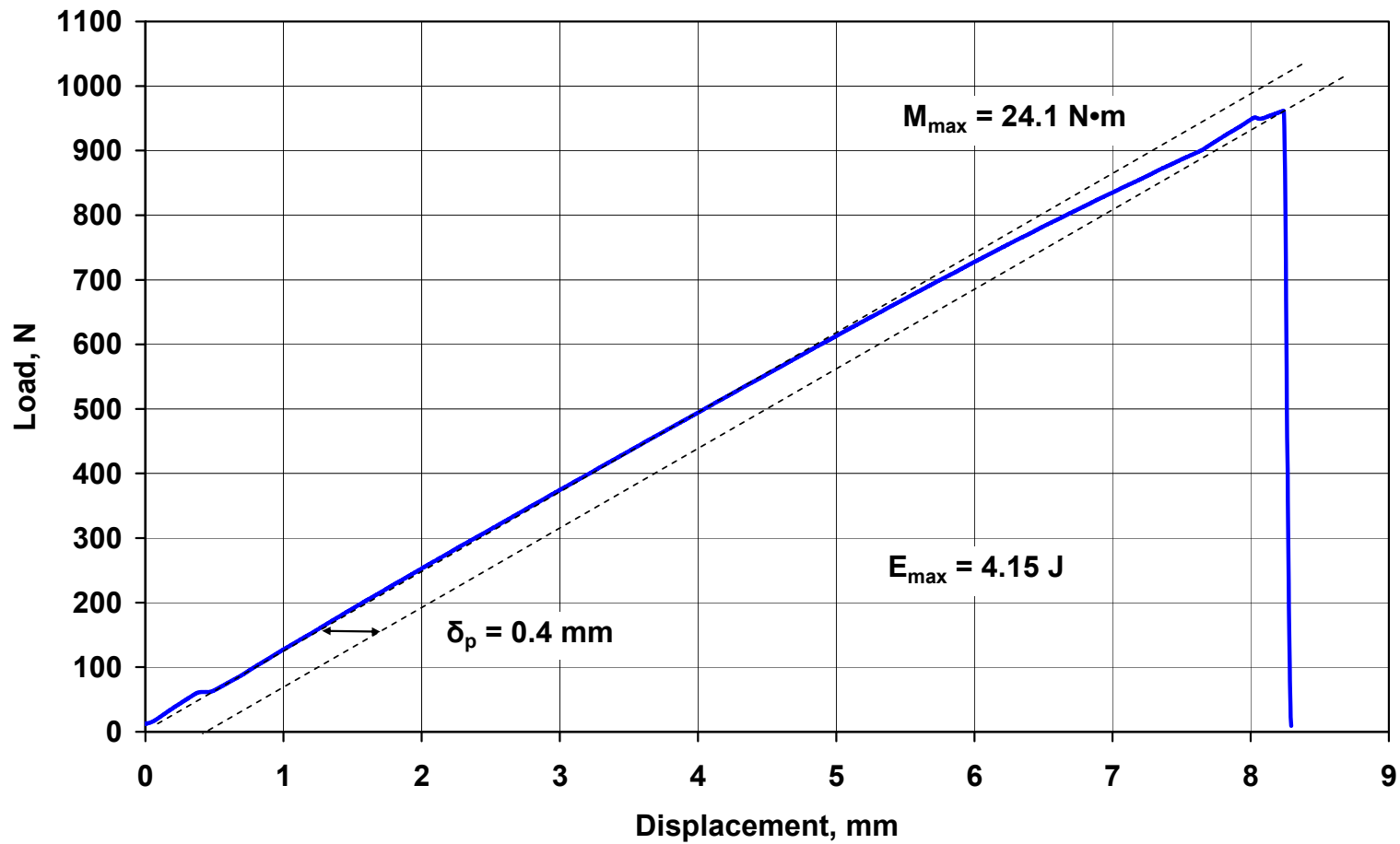


Fig. 12. Load-displacement curve for the OCZL#24 unpressurized LOCA sample oxidized one-sided to 17% CP-ECR, quenched at 800°C and subjected to four-point bending at 135°C and 1 mm/s displacement rate. The sample severed at two locations ( $\pm 38$  mm from the mid-span) following plastic deformation.



Fig. 13. Failure locations for the non-pressurized, one-sided-oxidized OCZL#24 sample (17% CP-ECR) following bending at 135°C and 1 mm/s. The 76-mm-long segment between the severed cross sections was used to section one metallographic sample and three 8-mm-long rings for RCT.

Table 3. Results of characterization and ring-compression testing (at 135°C and 2 mm/minute displacement rate) for the post-bend OCZL#24 sample that was oxidized (one-sided) to 17% CP-ECR

<b>Parameters</b>	<b>Value</b>
Oxidized Cladding OD, mm	9.73±0.02
OD Oxide Layer Thickness, μm	103±9
Average Metal Wall Thickness, mm	0.50
Average Metal ID, mm	8.52
RCT Offset Displacement, mm	0.18 0.11 <u>0.13</u> 0.14±0.04
RCT Offset Strain, %	1.9 1.2 <u>1.4</u> 1.5±0.4
RCT Permanent Displacement, mm	0.11 0.07 <u>0.08</u> 0.09±0.02
RCT Permanent Strain, %	1.2 0.7 <u>0.8</u> 0.9±0.3

## **Appendix A**

### **Load-Displacement Curves for Post-LOCA Bend Samples OCZL#19 through #29**

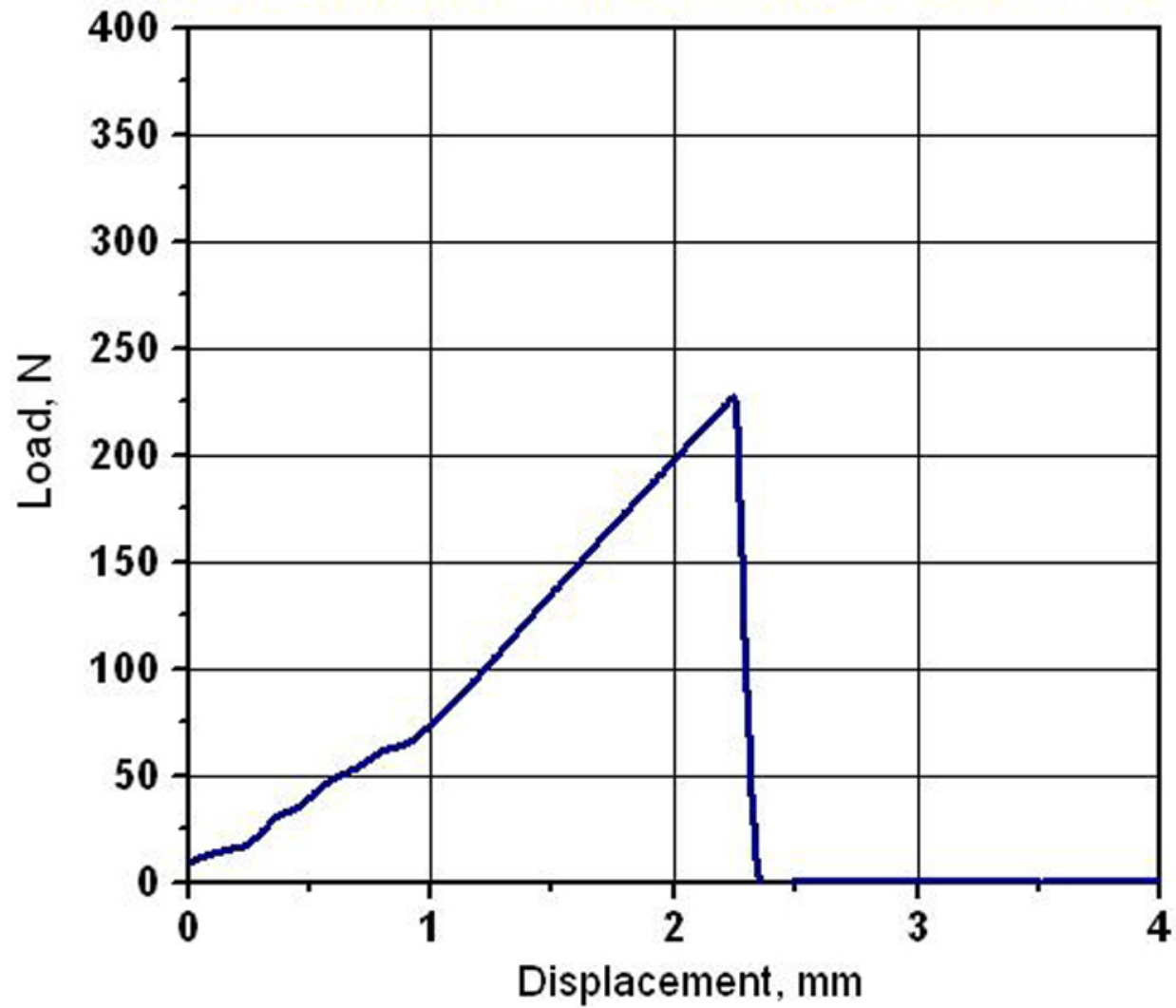


Fig. A.1 Load-displacement curve for post-LOCA sample OCZL#19 (17% CP-ECR) subjected to bending at 135°C and 2 mm/s displacement rate with the rupture tips under maximum tensile stress. Sample severed at two locations ( $\pm 23$  mm from rupture mid-span) in higher hydrogen regions.

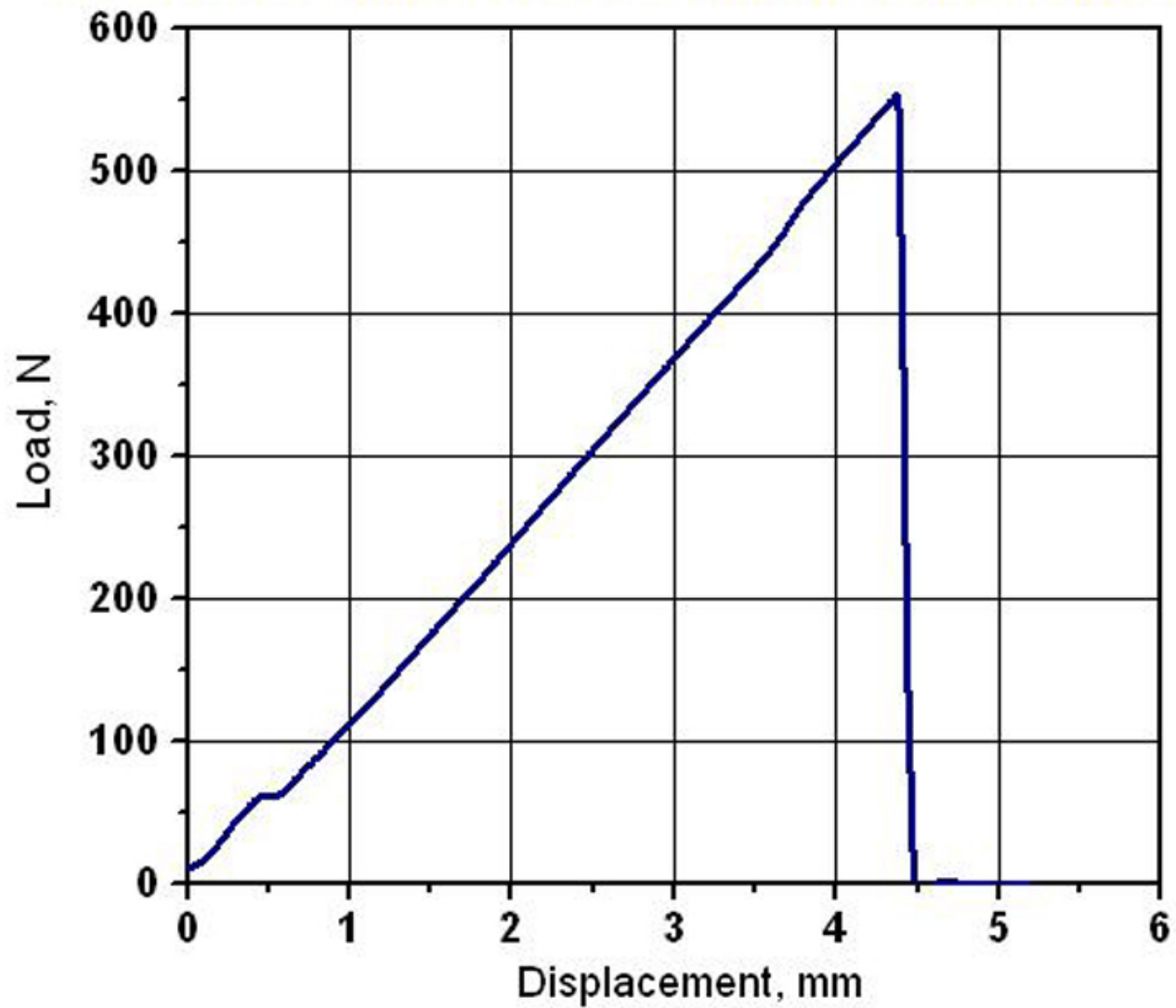


Fig. A.2 Load-displacement curve for post-LOCA sample OCZL#21 (10% CP-ECR) subjected to bending at 135°C and 2 mm/s displacement rate with the rupture tips under maximum tensile stress. Sample severed at two locations (-29 mm and +33 mm from rupture mid-span) in higher hydrogen regions.

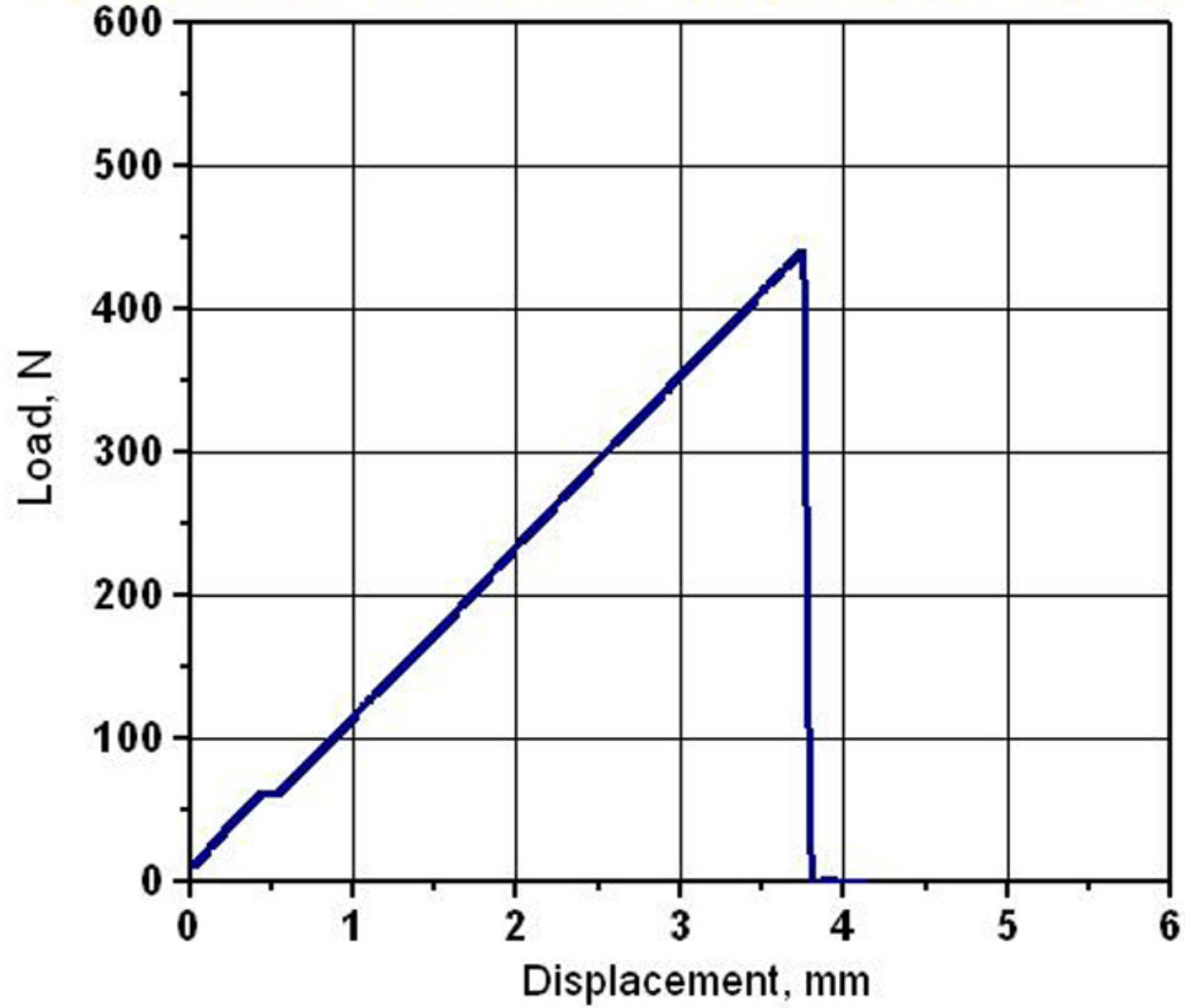


Fig. A.3 Load-displacement curve for post-LOCA sample OCZL#22 (11% CP-ECR) subjected to bending at 135°C and 1 mm/s displacement rate with the rupture tips under maximum tensile stress. Sample severed at two locations (-27 mm and +35 mm from rupture mid-span) in higher hydrogen regions.

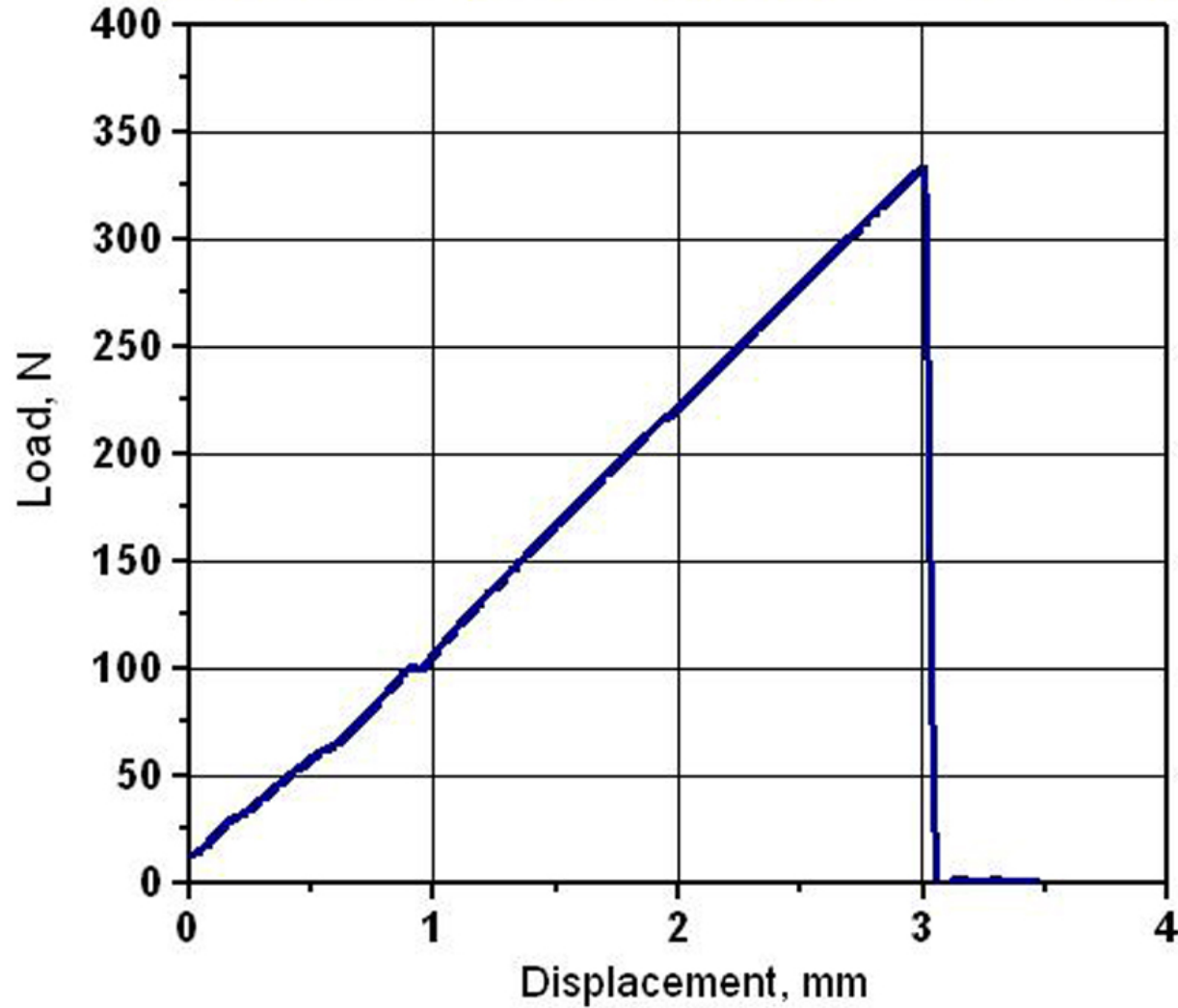


Fig. A.4 Load-displacement curve for post-LOCA sample OCZL#25 (16% CP-ECR) subjected to bending at 135°C and 1 mm/s displacement rate with the rupture tips under maximum tensile stress. Sample severed at two locations ( $\pm 26$  mm from rupture mid-span) in higher hydrogen regions.

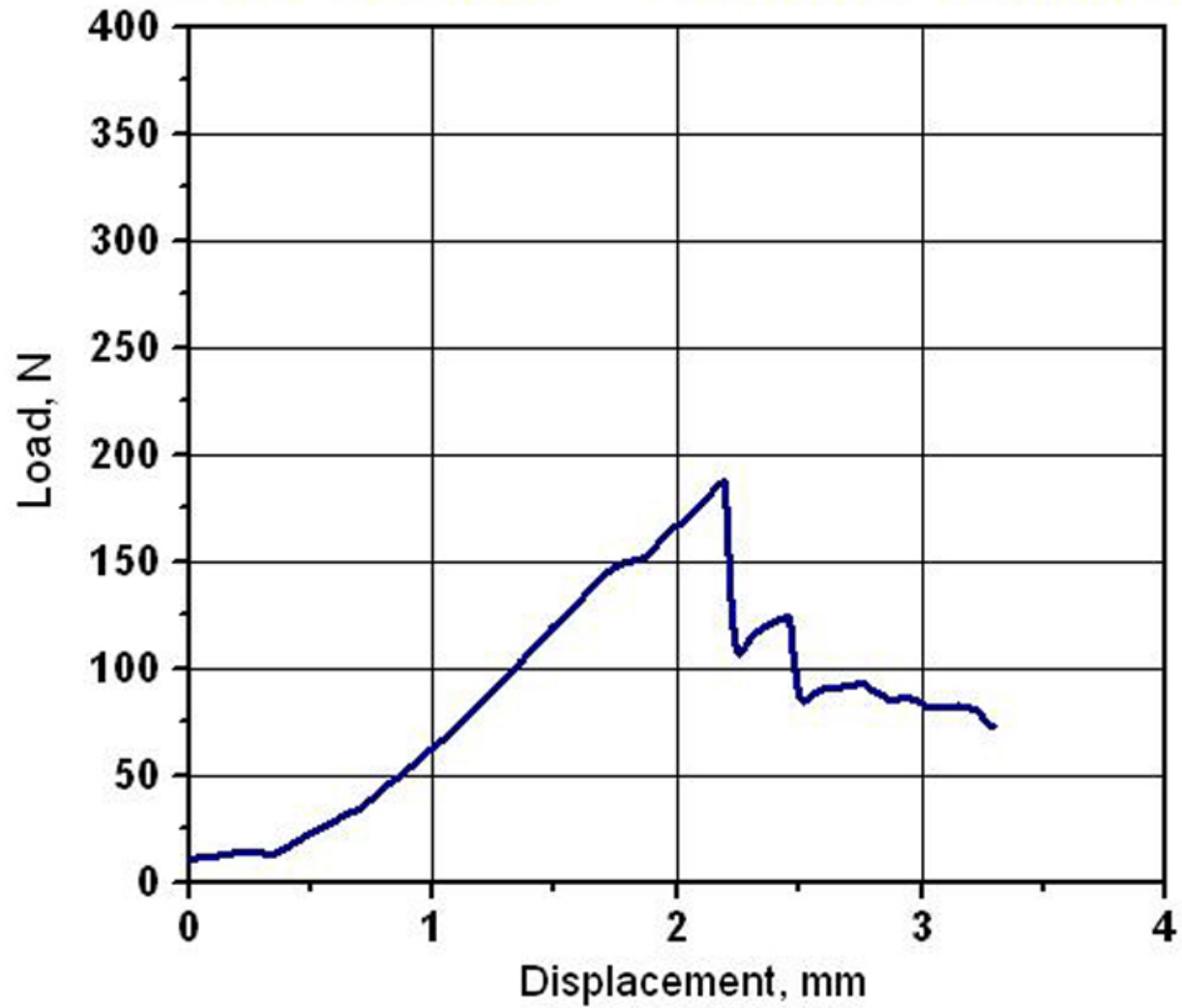


Fig. A.5a Load-displacement curve for post-LOCA sample OCZL#29 (17% CP-ECR) subjected to bending at 135°C and 1 mm/s displacement rate with the rupture tips under maximum tensile stress. Test was interrupted to measure a crack through the rupture node that extended through 60% of the cross section.

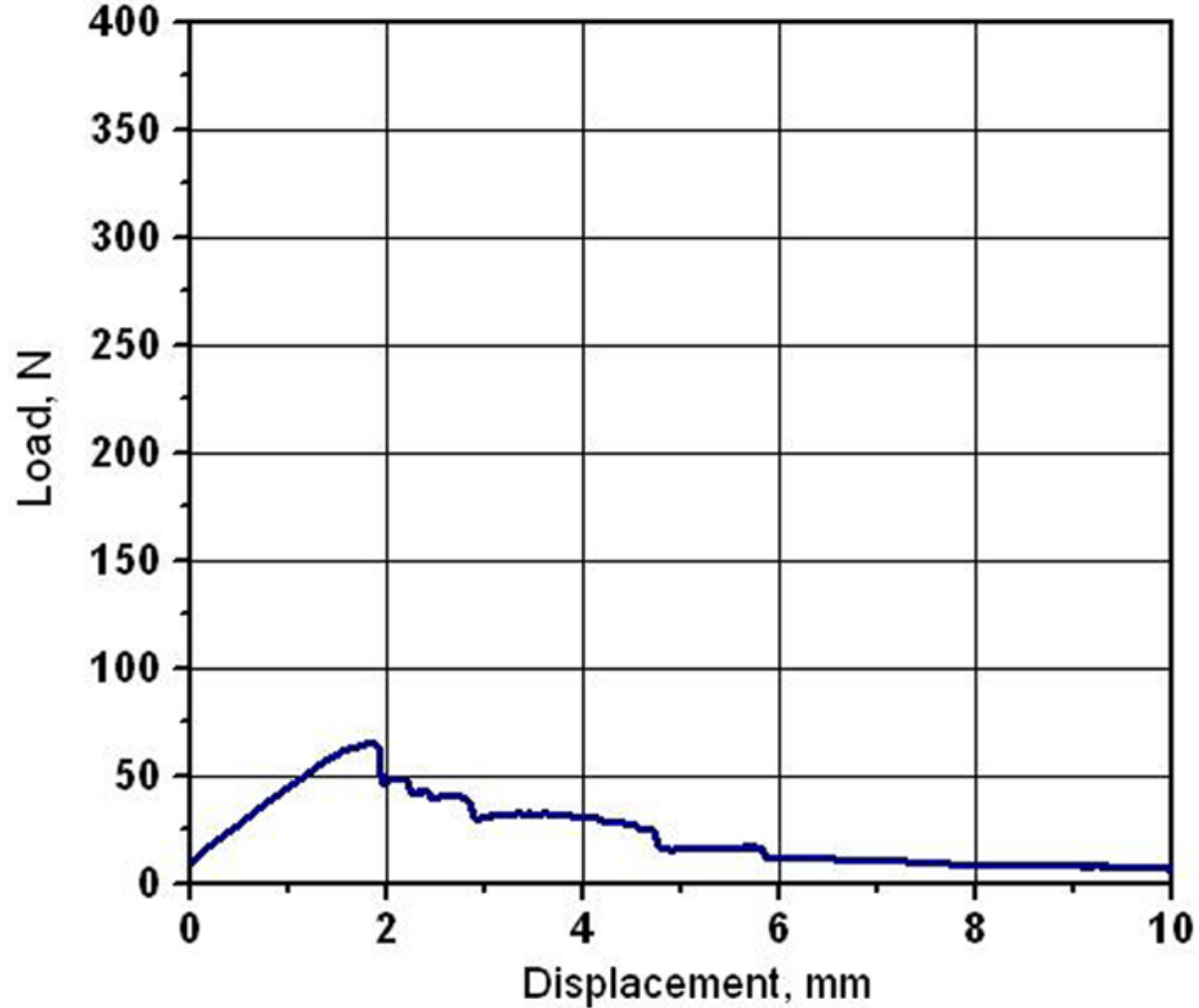


Fig. A.5b Load-displacement curve for post-LOCA sample OCZL#29 (17% CP-ECR) subjected to bending at 135°C and 1 mm/s displacement rate with the rupture tips under maximum tensile stress. Following this reloading of the sample, the crack extended from 60% to 90% of the cross section. However, the sample was intact at the end of the test following significant plastic deformation.